Optoelectronic properties of hydrogenated amorphous germanium deposited by rf-PECVD as a function of applied rf-power

2005 J. Phys.: Condens. Matter 17 5149

(http://iopscience.iop.org/0953-8984/17/33/017)

INSTITUTE OF PHYSICS PUBLISHING JOURNAL OF PHYSICS: CONDENSED MATTER

J. Phys.: Condens. Matter **17** (2005) 5149–5158 doi:10.1088/0953-8984/17/33/017

Optoelectronic properties of hydrogenated amorphous germanium deposited by rf-PECVD as a function of applied rf-power

Y Bouizem, A Belfedal[1], J D Sib, A Kebab and L Chahed

Laboratoire de Physique des Couches Minces et Matériaux pour l'Electronique, Université d'Oran, Es-Sénia 31100, Algeria

E-mail: aekbelfedal2002@yahoo.fr

Received 18 May 2005, in final form 15 July 2005
Published 5 August 2005
Online at stacks.iop.org/JPhysCM/17/5149

Abstract

This paper is devoted to the optoelectronic properties of hydrogenated amorphous germanium (a-Ge:H) deposited by the plasma-enhanced chemical vapour deposition (PECVD) technique on the powered electrode under different applied radio frequency power (rf-power) in a conventional, parallel plate reactor. This study investigates in more detail the density of states of the material by analysing the optical absorption spectra obtained by combining optical measurements, photothermal deflection spectroscopy (PDS) and constant photocurrent method (CPM) techniques. The PDS and CPM results are in good agreement. The disorder parameter in optimized samples ($E_{0\,\mathrm{V}} \sim 42$ meV) seems to be the lowest reported to date. However, the deep-gap states density N_{D} is higher in optimized a-Ge:H than in optimized hydrogenated amorphous silicon (a-Si:H) by more than an order of magnitude.

1. Introduction

Hydrogenated amorphous silicon (a-Si:H) based binary alloys are always a subject of much interest in the development of high-quality photovoltaic solar cells which require narrow band-gap materials. It is generally admitted that the optical band-gap of a-Si:H is easily narrowed by adding to the amorphous silicon network atoms of germanium [1]. As a consequence, there is a sharp deterioration of the electronic properties of hydrogenated amorphous silicon–germanium alloys (a-Si–Ge:H) with an increasing Ge concentration [1] which is not well understood yet. So, instead of approaching the a-Si–Ge:H film deposition problem as a perturbation of the standard conditions which produce high-quality a-Si:H, many authors [2, 3] have suggested that the photo-response of a-Si–Ge:H alloys can be improved by the optimization of the deposition methods leading to high electronic quality a-Ge:H films similar to that already reached for

[1] Author to whom any correspondence should be addressed.

a-Si:H, and also through proper understanding of their optoelectronic properties. In this view and in order to approach this methodology, a large amount of results obtained on optimized a-Ge:H films deposited by different techniques has been published. In particular, it has been reported by Godet *et al* [4, 5] that some properties, such as disorder, in a-Ge:H thin films produced on the grounded anode by the plasma enhanced-chemical vapour deposition (PECVD) technique are strongly improved when germane gas (GeH_4) is diluted at 1% in H_2 under some optimized plasma conditions and under the so-called 'standard' deposition conditions, (i.e., low rf-power and low pressure). However, these standard deposition conditions result in a low deposition rate ($r_d \sim 0.5$ Å s^{-1}). On the other hand, Wetsel *et al* [6], Turner *et al* [7] and Wickboldt *et al* [8] have shown that the optoelectronic properties of a-Ge:H deposited by the PECVD technique on the powered electrode (cathode) were dramatically superior to those films deposited on the unpowered electrode (anode) where device-quality a-Si:H is conventionally deposited. The differences in film growth and structure observed in the cathode-deposited a-Ge:H compared to the anode-deposited a-Ge:H have been largely discussed by these authors and attributed mainly to the high ion bombardment energy at the cathode surface.

The present study reports on the optoelectronic properties of a-Ge:H films deposited on the powered electrode. In particular, the effect of the rf-power was investigated on the deposition rate and the electronic parameters by combining optical measurements, photothermal deflection spectroscopy (PDS) [9] and constant photocurrent method (CPM) [10] techniques. The comparison between the results obtained by the two techniques is also discussed.

2. Experimental details

The a-Ge:H films used in this study were deposited by PECVD of a mixture of germane and hydrogen gases in the reactor described elsewhere in the literature [8]. The samples were deposited on the powered electrode (diameter = 5.7 cm and 1.4 cm gap spacing between the electrodes) of the system with 13.56 MHz signal and at different applied rf-power ranging from 12 to 48 W (table 1). The chamber pressure was regulated at 0.95 torr and the substrate temperature was maintained at 200 °C. The gas flows were 1.00 sccm GeH_4 diluted with 40.00 sccm H_2.

Infrared (IR) transmission measurements were performed on a-Ge:H films deposited on roughened crystalline silicon substrates to derive the vibrational absorption spectra in the frequency range 400–2400 cm^{-1} and to obtain the total bonded hydrogen content C_H. The thickness d, the band gap parameters E_{04}, defined as the energy at which the absorption coefficient α is equal to 10^4 cm^{-1} (with a 0.01 eV absolute error), the static refractive index n_0, the average gap E_m as well as the dispersion energy E_w were determined from standard optical transmission (OT) measurements performed on the films deposited simultaneously on Corning 7059 glass substrates. PDS and CPM techniques were used to determine accurately the sub-band gap absorption $\alpha(\hbar\omega)$ down to quite low energies. The analysis of the derived spectra allows us to derive the main parameters characterizing the density of states (DOS) distribution within the mobility gap, in particular the deep defect density N_D and the valence-band tail width E_{0V} (parameter characteristic of the disorder and the distorted or weak Ge–Ge bonds).

3. Results and discussion

3.1. Deposition kinetics

It has been frequently reported that the rf glow discharge decomposition of germane diluted in hydrogen at low rf-power and low pressure is the most widely used technique for optimized

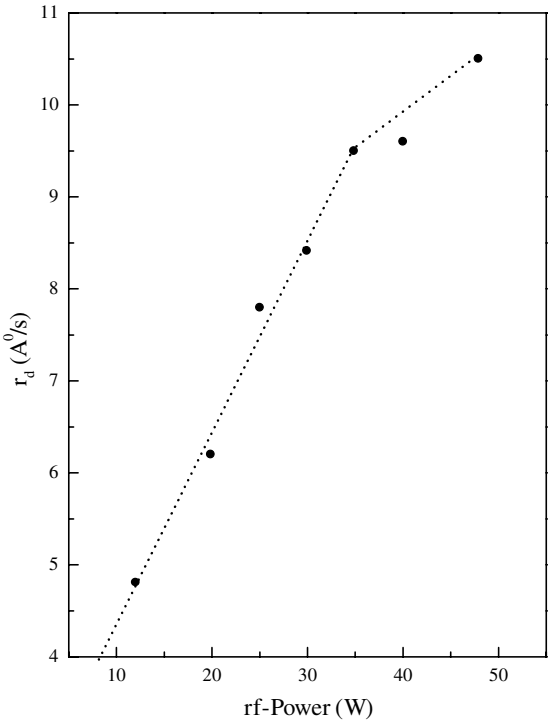

Figure 1. Deposition rate r_d as a function of the applied rf-power.

a-Ge:H deposition. However, the standard deposition conditions lead to a low deposition rate ($r_d \sim 0.5$ Å s^{-1}) which constitutes a serious drawback in applications when thick films are desired. Therefore increase of r_d in the a-Ge:H film preparation without degradation of the optoelectronic properties of the material is required. In this study the increase of r_d up to 10.5 Å s^{-1} has been reached by operating the discharge in the high-pressure and high rf-power regime. Figure 1 presents the effect of the applied rf-power on r_d (obtained from the ratio of the film thickness to the deposition time). It can immediately be seen that r_d increases linearly with increasing rf-power from 12 to 35 W. This behaviour can be explained by the fact that in the high rf-power regime the discharge becomes resistive and the rf energy is more efficiently coupled to the plasma through the bulk electrons which gain energy from the electric field produced in the inter-electrode space [11]. As a result, more radicals are dissociated in the discharge and reach the grounded electrode with a high sticking coefficient. At the highest powers (rf-power >35 W) the r_d appears to increase more slowly up to ∼10.5 Å s^{-1}. This effect can be explained by the possibility of heavily diluted germane gas being fully dissociated at these powers, and so the addition of further rf-power cannot increase gas utilization.

3.2. Structural and optical properties

The IR absorption spectrum for a non-optimized sample deposited at 48 W is represented in figure 2. This spectrum fits a general picture already reported for the cathode deposited a-Ge:H since no peak at 860 cm^{-1}, corresponding to contamination with oxygen, is observed after several hours of air exposure [7]. The stretching band shows beside the main Ge–H band centred at 1875 cm^{-1} a relatively large contribution centred at 1975 cm^{-1}. This component can be related to the distinct bending band consisting of two well resolved peaks centred at

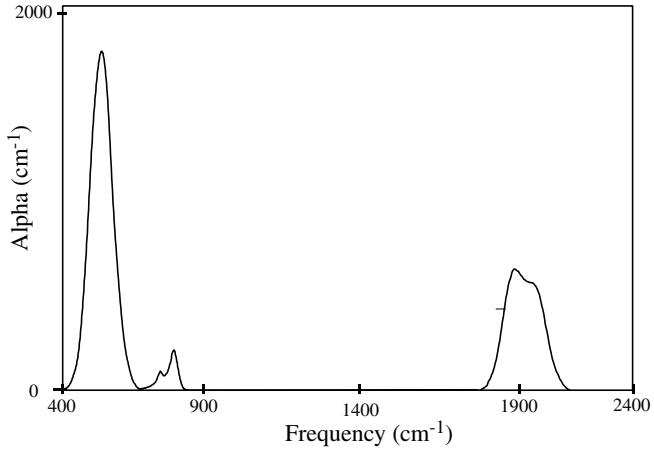

Figure 2. Infrared absorption spectrum for the sample prepared at rf-power of 48 W.

about 760 and 830 cm^{-1} respectively, and indicates a significant proportion of $(GeH_2)_n$ groups. The corresponding absorption band at 2090 cm^{-1} [12, 13] in a-Si:H is often accepted as being incompatible with good electronic properties. This is indeed verified here, as discussed in section 3.3. When the rf-power is decreased to 25–30 W (optimized samples), the stretching band essentially consists of a single band centred at 1875 cm^{-1}, which shows that the hydrogen is mainly incorporated as isolated monohydride Ge–H groups. In addition to this type of inference, the total bonded hydrogen content C_H is obtained from the integrated area I_ω under the absorption band corresponding to the Ge–H wagging mode centred at 560 cm^{-1} [14]:

$$N_H(cm^{-3}) = A_\omega I_\omega = \omega \int \frac{\alpha(\omega)}{\omega}\, d\omega \tag{1}$$

where $\alpha(\omega)$ is the absorption coefficient of the film at frequency ω, and $A_\omega = 1.6 \times 10^{19} cm^{-2}$ is the proportionality factor for this band, obtained by the calibration of N_H (cm^{-3}) against the hydrogen content deduced by the nuclear reaction technique. The percentage of hydrogen C_H in the films was then deduced from the following relation:

$$C_H(at.\%) = \frac{A_\omega I_\omega}{\rho_{c-Ge}} \times 100 \tag{2}$$

where $\rho_{c-Ge} = 4.5 \times 10^{22}$ cm^{-3} is the atomic density of crystalline germanium. Experimental errors in the analysis of the IR measurements result mainly from the determination of the base line of the spectrum and from the determination of the film thickness. An error of about 1 at.% is estimated on the evaluation of C_H. The values of C_H deduced from this analysis and typical parameters characteristic of the samples deduced from OT measurements are listed in table 1. An important remark can be made immediately from these data. It can be seen that the rf-power has little effect on the variation of C_H since the values remained at (5.5 ± 1) at % except for the sample deposited at higher rf-power (48 W), i.e. at higher r_d. Figure 3 is a plot of the band-gap parameters E_{04} as a function of rf-power. It can be seen that E_{04} increases linearly as the rf-power increases from 12 to 25 W and remains constant above 25 W. It is too difficult to attribute the E_{04} variation to an explicit alloying effect with hydrogen, since no variation of C_H within experimental error is observed in these samples. The observed trends may be correlated to the microstructure of the material. But the small changes expected in the relative IR absorption peak heights around 800 cm^{-1} cannot be observed since the determination of

Table 1. The rf-power characteristics of the samples. The deposition rate r_d was obtained from the ratio of the film thickness to the deposition time. The hydrogen content C_H was derived from the infrared absorption band at 560 cm^{-1}. The thickness d, the band-gap parameters E_{04}, the static refractive index n_0, the average gap E_m and the dispersion energy E_w were deduced from optical transmission measurements.

rf-power (W)	r_d (Å s^{-1})	C_H (at.%)	d (μm)	E_{04} (eV)	n_0	E_m (eV)	E_w (eV)
12	4.8	4.4	3.12	1.19	4.23	2.34	46
20	6.2	4.6	2.13	1.22	4.17	2.53	45
25	7.8	5.5	1.93	1.25	4.11	2.60	43
30	8.4	4.9	1.94	1.25	4.10	2.59	41
35	9.5	5.9	2.06	1.25	4.04	2.59	40
40	9.6	6.1	1.57	1.25	4.01	2.58	39
48	10.5	7.7	1.19	1.25	3.96	2.59	38

the base line is usually affected by interference fringes. In fact, the existence of a relationship between a small-range structure and a-Ge band-gap has been frequently asserted [15]. In order to understand this phenomenon well, the variation of the static refractive index n_0 is deduced from the analysis of the Wemple–Didominico one-oscillator model [16], and analysed as a function of rf-power. According to this model, the dispersion relation of the refractive index is given by

$$n^2(\hbar\omega) = 1 + \frac{E_w E_m}{E_m^2 - (\hbar\omega)^2} \tag{3}$$

where E_w denotes the dispersion energy related to the coordination number of the atoms and E_m defines the average gap usually considered as the energy separation between the centres of both the conduction and the valence bands. The static refractive index n_0, E_m and E_w are determined by considering the variation of $[n^2(\hbar\omega) - 1]^{-1}$ as a function of $(\hbar\omega)^2$; the deduced values are listed in table 1. The increase of the average gap E_m (which has the same trends as E_{04}) can be correlated with the decrease of n_0 in the range 12–25 W according to the formula derived by Penn [17]:

$$n_0^2 = 1 + A\frac{(\hbar\omega_p)^2}{E_m^2} \tag{4}$$

where $\hbar\omega_p$ is the plasma energy for valence electrons and A is a parameter depending on the matrix element. Above this range, n_0 diminishes while no change is observed in E_m and E_{04} values. This variation suggests that the increase of rf-power is accompanied with a little microstructure and a small density loss in the material. The values of the dispersion energy E_w show the same trends as n_0 and suggest a decrease in the average coordination number of the atoms.

Since the values of n_0 and E_w remain high in all of the range of rf-power variation, and no oxygen contamination is revealed by the IR transmission spectra, we speculate that the particular microstructure of these films is not of the 'island and tissue' type [18] but may rather consist in a dense matrix with small isolated voids within the network with a low hydrogen content.

3.3. Subgap absorption

In this section the density of states of the material is investigated in detail by analysing carefully the optical absorption spectra obtained as explained before from a combination of PDS, CPM

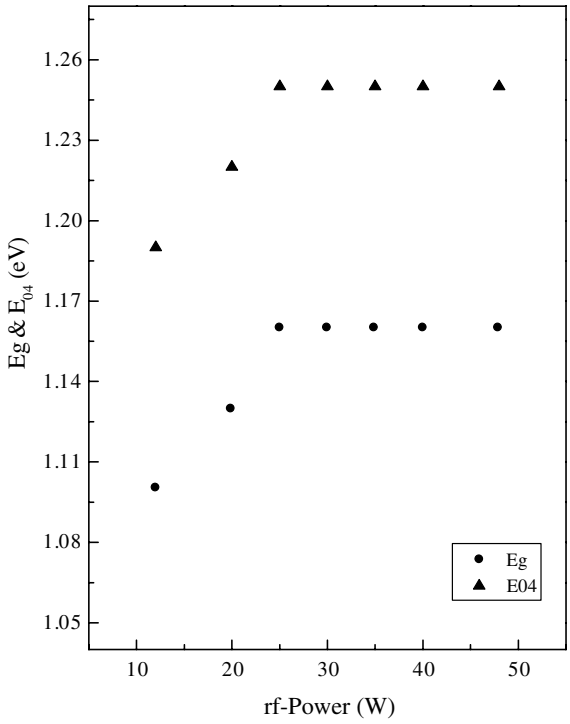

Figure 3. Band-gap parameters E_{04} as a function of the applied rf-power. The mobility gap E_g is also represented for comparison. The difference between E_{04} and E_g remains practically the same at a value of 0.09 eV.

and OT measurements. The PDS-derived spectra are normalized to absolute values by matching the Urbach edge region with the optical absorptance spectra deduced from OT measurements in the high-energy range [19]. Then, according to our procedure proposed recently [20], the optical absorption coefficient $\alpha(\hbar\omega)$ is determined from the ratio of the normalized PDS spectra to the transmittance ones. The CPM spectra are then carefully calibrated by fitting to the entire optical absorption coefficient spectra $\alpha(\hbar\omega)$ [21]. Using this method to calibrate CPM spectra is more accurate and offers the enormous advantage to have a large overlap range between the spectra. An example of such a calibration is given in figure 4. It can clearly be seen that there is a perfect agreement between the PDS- and the CPM-derived spectra in the Urbach edge region over more than one decade. This result suggests that both PDS and CPM techniques detect the same optical transitions in this range. In the high-energy range the CPM spectrum deviates from the $\alpha(\hbar\omega)$ spectrum because, in this range, surface recombination limits the photocurrent as the light penetration depth decreases with increasing $\alpha(\hbar\omega)$. In the low-energy range the CPM spectrum falls below the PDS spectrum because the PDS technique probably probes more optical transitions and absorption surface [22] which the CPM technique cannot detect. This problem is not well understood and will not be considered in this study.

Some characteristic parameters of the material can be derived from the analysis of these spectra at low energies. The apparent Urbach energy $E_{0\mathrm{app}}$, characterizing the disorder and the distorted or weak Ge–Ge bonds, is usually determined by a linear regression of the exponential data range. However, the contribution of the deep defect absorption in this range may increase this parameter, in particular for the non-optimized samples. For the same reason the deep defect density obtained by integrating the excess absorption above the exponential edge, which is the

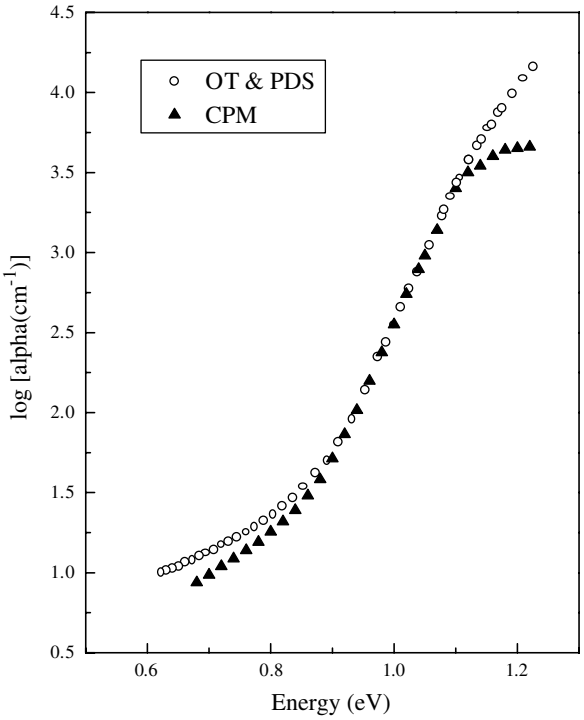

Figure 4. Calibration of a CPM spectrum by fitting to the entire optical absorption coefficient spectrum deduced from optical and PDS measurements.

usual procedure for a-Si:H [9], is strongly underestimated. For obtaining more correct values of the disorder parameter $E_{0\,\mathrm{V}}$ and the deep defect density N_{D}, the optical absorption spectra are analysed by using the deconvolution procedure proposed recently by Bouizem *et al* [23]. A good fit to the data was obtained with a Gaussian distribution for the deep-gap states centred at $E_{\mathrm{D}} = (0.60 \pm 0.02)$ eV below the conduction-band mobility edge, with a full width at half maximum equal to 0.32 ± 0.02 eV. The values of the mobility gap E_{g}, and the values of $E_{0\,\mathrm{V}}$ and N_{D} deduced from this analysis are listed in table 2. The values of the mobility gap E_{g} correlate well with those of E_{04} and its variation as a function of rf-power shows the same trends (figure 3). The 'true' $E_{0\,\mathrm{V}}$ values obtained by this procedure are not influenced, as explained before, by the contribution from the deep-gap states absorption in the Urbach-tail range. They differ by about 2 meV only for the optimized samples and about 12 meV for the worst sample (with the highest deep-states absorption) from the 'apparent', $E_{0\mathrm{app}}$, ones. Since the PDS- and the CPM-derived absorption spectra corroborate very well in the Urbach edge region, the deconvolution of these spectra leads to the same $E_{0\,\mathrm{V}}$ values with 1 meV absolute uncertainty ascribed to the errors in both determinations. Also, it must be noticed that the $E_{0\,\mathrm{V}}$ as well as the $E_{0\mathrm{app}}$ values obtained here for the optimized samples are smaller than those of high-quality a-Ge:H or a-Si:H reported in the literature [4, 7, 24]. As expected, the values of the deep defect density N_{D} obtained from the analysis of PDS-derived spectra are systematically higher than the corresponding values deduced from the analysis of CPM-derived spectra. This difference can be attributed to additional contributions from optical transitions which are not detected in CPM measurements and probably to additional absorption of a defective surface and/or interface layers detected by PDS measurements [22]. Figures 5 and 6

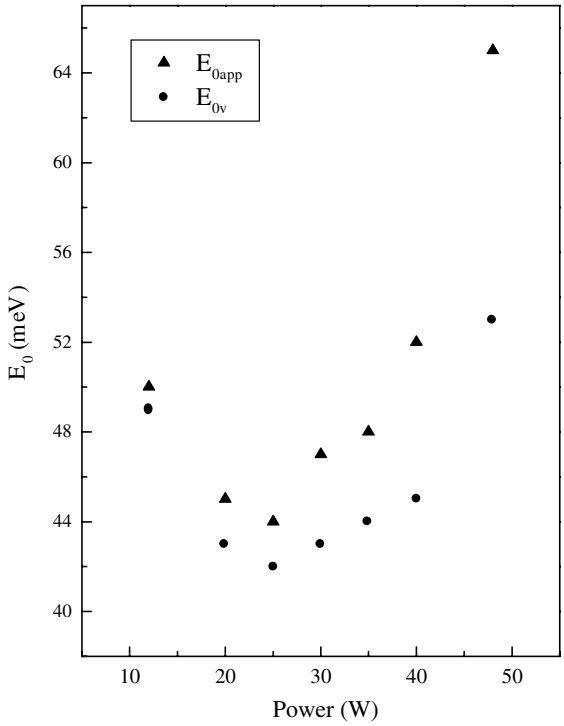

Figure 5. The disorder parameter $E_{0\mathrm{app}}$ and $E_{0\,\mathrm{V}}$ as a function of applied rf-power.

Table 2. The mobility gap E_{g}, the disorder parameter $E_{0\,\mathrm{V}}$, and the deep defect density N_{D} deduced from the decomposition procedure given in section 3.2. The apparent Urbach energy $E_{0\mathrm{app}}$ values are also reported for comparison.

r.f-power (W)	E_{g} (eV)	$E_{0\,\mathrm{V}}$ (meV)	$E_{0\mathrm{app}}$ (meV)	N_{D} ($\times 10^{16}$ cm^{-3}) PDS	CPM
12	1.10	49	50	28	17
20	1.13	43	45	25	8
25	1.16	42	44	18	4
30	1.16	43	47	21	5.5
35	1.16	44	48	20	5.2
40	1.16	45	52	37	7.5
48	1.16	53	65	130	12

show respectively the variations of the disorder parameter and the deep defect density N_{D} with rf-power. It can be seen that all the parameters obtained by both PDS and CPM techniques follow roughly the same trends in the whole rf-power range; they present an optimum in the 25–30 W range. The remarkable improvement of these parameters in this range is most readily attributed to high ion bombardment energy at the cathode surface, to a better surface passivation by the hydrogen atoms during the film growth, and to the hydrogen incorporated mainly as Ge–H bonds which is effective in reducing Ge network distortion by substituting for overconstrained Ge–Ge bonds and in saturating the dangling bonds. The quality of the films eventually deteriorates as the rf-power increases and becomes too high (rf-power >35 W). This

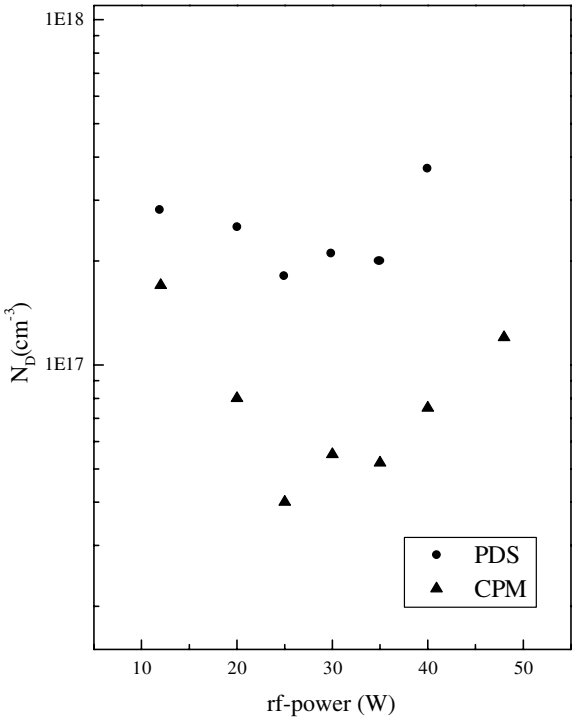

Figure 6. The deep defect density N_D deduced from the analysis of the PDS- and the CPM-derived spectra as a function of the applied rf-power.

high rf-power regime influences the nature and concentration of various species present in the plasma which play a dominant role in the deposition kinetics and are ultimately responsible for the film growth. The degradation of the material properties to its inhomogeneous structure is correlated to the $(GeH_2)_n$ groups as shown by the IR absorption spectra, and to the loss in the density of the material as revealed by the variations of the static refractive index and the dispersion energy.

Despite the lowest values of the disorder parameter obtained here for the optimized a-Ge:H, the deep-gap states density remains higher by more than an order of magnitude than in a-Si:H device quality [24]. The high value of a-Ge:H deep-gap states density can be quantitatively explained by the thermal equilibrium model proposed by Smith and Wagner for a-Si:H [25] as has been suggested in our earlier work [26].

4. Conclusion

In this paper, special attention was paid to the analysis of PDS- and CPM-derived optical absorption spectra obtained down to quite low energies on a-Ge:H films deposited on the powered electrode. The mobility gap, the disorder parameter and the deep-defect density were analysed by a suitable deconvolution procedure applied to optical absorption coefficient spectra. The PDS and the CPM results obtained are in very good agreement. The values of the disorder parameters ($E_{0V} \sim 42$ meV) obtained seem to be the best reported to date. However, the deep-gap states density N_D is higher in the optimized a-Ge:H than in optimized a-Si:H by more than an order of magnitude.

Acknowledgments

The authors wish to thank Dr M L Thèye for many helpful discussions and Professor W Paul for providing the samples used in this study.

References

[1] Chou Y-P and Lee S-C 1998 *J. Appl. Phys.* **83** 4111
[2] Karg F H, Böhm H and Piertz K 1989 *J. Non-Cryst. Solids* **114** 477
[3] Jones S J, Lee S M, Turner W A and Paul W 1989 *Mater. Res. Soc. Symp. Proc.* **149** 45
[4] Godet C, El Zawawi I, Thèye M L, Gauthier M and Stoquert J P 1990 *Solid State Commun.* **74** 721
[5] Godet C, Chu V, Equer B, Bouizem Y, Chahed L, El Zawawi I, Thèye M L, Basrour S, Bruyère J C and Stoquert J P 1990 *Amorphous Silicon Technology* (*MRS Symp. Proc. No 192*) ed P C Taylor, M J Thompson, P G Le Comber, Y Hamakawa and A Madan (Pittsburgh, PA: Materials Research Society) p 163
[6] Wetsel A E, Jones S J, Turner W A, Pang D, Paul W, El Zawawi I, Bouizem Y, Chahed L, Thèye M L, Marques F C and Chambouleyron I 1990 *Amorphous Silicon Technology* (*MRS Symp. Proc. No 192*) ed P C Taylor, M J Thompson, P G Le Comber, Y Hamakawa and A Madan (Pittsburgh, PA: Materials Research Society) p 547
[7] Turner W A, Jones S J, Pang D, Bateman B F, Chen J H, Li Y M, Marques F C, Wetsel A E, Wickboldt P, Paul W, Bodart J, Norberg R E, El Zawawi I and Thèye M L 1990 *J. Appl. Phys.* **67** 7430
[8] Wickboldt P, Jones S J, Pang D, Turner W A, Wetsel A E, Paul W and Chen J H 1991 *Phil. Mag.* B **64** 655
[9] Amer N M and Jackson W B 1984 *Semiconductors and Semimetals* vol 21B, ed J I Pankove (New York: Academic) p 83
[10] Vanecek M, Kocka J, Stuchlik J, Kozisek Z, Stika O and Triska A 1983 *Sol. Energy Mater.* **8** 411
[11] Bohm C and Perrin J 1991 *J. Phys. D: Appl. Phys.* **24** 865
[12] Bermejo D and Cardona M 1979 *J. Non-Cryst. Solids* **32** 421
[13] Freeman E C and Paul W 1978 *Phys. Rev.* B **18** 4288
[14] Fang C J, Gruntz K J, Ley L and Cardona M 1980 *J. Non-Cryst. Solids* **35** 255
[15] Paul W, Connell G A N and Temkin R J 1973 *Adv. Phys.* **22** 529
[16] Wemple S H and Didomenico M 1971 *Phys. Rev.* B **3** 1338
[17] Penn D R 1962 *Phys. Rev.* **128** 2093
[18] Paul W 1988 *Amorphous Silicon and Related Materials* vol 1A, ed H Fritsche (Singapore: World Scientific) p 63
[19] Thèye M L, Chahed L, Rocca i Cabarrocas P and Zellama K 1991 *Phil. Mag.* B **63** 143
[20] Bouizem Y, Belfedal A, Sib J D and Chahed L 2000 *Opt. Commun.* **178** 111
[21] Slàdek P, Bouizem Y, Thèye M L and Rocca i Cabarrocas P 1993 *Proc. 11th E.C. Photovoltaic Solar Energy Conf.* ed L Guimaraes, W Palz, C de Reyff, H Kiess and P Helm (Switzerland: Harwood Academic) p 710
[22] Chahed L, Thèye M L, Fournier D, Roger J P, Boccara A C, Li Y M, Turner W A and Paul W 1991 *Phys. Rev.* B **43** 14488
[23] Bouizem Y, Belfedal A, Sib J D and Chahed L 2003 *Solid State Commun.* **126** 675
[24] Roca i Cabarrocas P, Bouizem Y and Thèye M L 1992 *Phil. Mag.* B **65** 1025
[25] Smith Z E and Wagner S 1987 *Phys. Rev. Lett.* **59** 688
[26] Godet C, Bouizem Y, Chahed L, El Zawawi I, Thèye M L, Meaudre M, Meaudre R, Basrour S and Bruyère J C 1991 *Phys. Rev.* B **44** 5506